will be avoided in real wind-tunnel testing. When all of these factors are taken into account, one can conclude that the SSMAW model, which dispenses with the more complex unsteady streamlining procedure required by the USLAW model, can be generally a useful adaptive wall model.

Conclusion

The existing SSFAW model is a reasonable means to reduce the wind-tunnel wall interference for the unsteady subcritical flow. However, the more sophisticated models such as SSMAW or USLAW are required for unsteady supercritical flows. The SSMAW model is an efficient wall model for both subcritical and supercritical flows provided we avoid testing near the wall resonance condition. The USLAW model produces the most accurate result, even near the resonance condition.

References

[1]Forshing, H., and Voss, R., "Adaptation for Unsteady Flow," *Adaptive Wind Tunnel Walls: Technology & Applications*, AGARD-AR-269, April 1990, pp. 91–99.

[2]Venkatakrishnan, V., and Jameson, A., "Computation of Unsteady Transonic Flows by the Solution of Euler Equations," *AIAA Journal*, Vol. 26, No. 8, 1988, pp. 974–981.

[3]Landon, R. H., "NACA 0012 Oscillator, and Transient Pitching," *Compendium of Unsteady Aerodynamic Measurement*, AGARD-R-702, Aug. 1982, pp. 3.1–3.25.

[4]Fromme, J. A., and Golberg, M. A., "Aerodynamic Interference Effects on Oscillating Airfoils with Controls in Ventilated Wind Tunnels," *AIAA Journal*, Vol. 18, No. 4, 1980, pp. 417–426.

Shock Oscillation in a Two-Dimensional, Flexible-Wall Nozzle

Shen-Min Liang,* Chou-Jiu Tsai,† and Fan-Ming Yu‡
National Cheng Kung University,
Tainan 701, Taiwan, Republic of China

Introduction

FLUID/STRUCTURE interaction problems are of great interest to aeronautical engineers, since some components of modern aircraft tend to be flexible to achieve high performance. In this Note, the interaction problem caused by inviscid transonic flow in a two-dimensional, convergent-divergent nozzle with flexible walls is considered.

Felker[1] studied the static aeroelastic problem by means of a direct method that solved the fully coupled discretized fluid dynamic and structural equations to obtain the equilibrium solution. His computed solution of wall pressure ahead of the throat agreed reasonably well with the test data of Mason et al.[2] But Felker's solution deviated from the test data downstream of the throat. Therefore, the objective of this paper is twofold. The first is to obtain a reasonably accurate (equilibrium) solution by establishing a proper spring model for representing the wall flexibility. Felker used a simple spring model in which the wall deformation was assumed to be linearly related to the difference between the local internal wall pressure and the ambient static pressure. The deformed wall shape was represented by a set of discrete displacements at selected nodes. The elastic spring constant k was assumed to be constant at each node. To achieve good accuracy, however, it is desirable to use a grid with grid points clustered near the throat. With Felker's spring model the nozzle wall may be too stiff at the throat region. To avoid this deficiency, the wall stiffness at each node is modified (described later) so that a more uniform wall elasticity is assured.

The second objective is to numerically investigate the transonic flow with shock oscillation caused by a downstream pressure fluctuation. Thus, the paper is an extension of our past research interest which was related to unsteady transonic flow with shock waves in a convergent-divergent channel with rigid walls.[3] The numerical simulation has been widely used for other aeroelastic problems.[4] The successful simulation of the two-dimensional problem is a stepping stone for studying three-dimensional aeroelastic nozzle problems.

Mathematical Formulation

Governing Equations

Without consideration of fluid flow viscosity and heat flux at the nozzle wall, the equations governing the nozzle flow with flexible walls are the time-dependent Euler equations.

Model of Wall Flexibility

The wall flexibility is represented by the discrete spring model described subsequently. The discrete displacement s at a selected node is assumed to be linearly related to the difference between the local internal wall pressure and the ambient static pressure. Unlike Felker's spring model, the elastic spring constant at node i, denoted by k_i, is set to be a constant $\bar{k}$ multiplied by a factor $w_i (<1)$ which is defined to be the ratio of the average of two adjacent element lengths, from point (x_i, y_i) to points (x_{i-1}, y_{i-1}) and (x_{i+1}, y_{i+1}) on the wall, to the total length of the nozzle wall. If w_i is set to be unity, the present spring model is reduced to Felker's model. The constant $\bar{k}$ is chosen such that the computed wall pressure matches the experimental data at some point.

Numerical Procedure

Discretization

The time-dependent Euler equations are discretized by a finite-volume approach associated with an improved implicit total-variation-diminishing (TVD) scheme of second order in time and space for unsteady flow calculation.[5] The present TVD scheme is basically the implicit TVD scheme of Yee and Harten[6] with an improved flux limiter.[5] The improved flux limiter allows the use of a larger Courant number for convergence. The discretized equations are solved with an approximate factorization of Beam and Warming[7] for computational efficiency.

Boundary Conditions

Flexible Wall

Since the nozzle wall is flexible, the wall surface can move outward or inward. Let $(\dot{x}_i, \dot{y}_i)$ be the wall velocity at node i at time t and s_i the wall displacement at node i from time t to time $t + \Delta t$. The wall velocity $(\dot{x}_i, \dot{y}_i)$ is determined by

$$\dot{x}_i = -\frac{s_i}{\Delta t}\frac{\Delta y_i}{d_i} \qquad \dot{y}_i = \frac{s_i}{\Delta t}\frac{\Delta x_i}{d_i}$$

where $(\Delta x_i, \Delta y_i)$ are defined as one-half of the coordinate differences between point (x_{i+1}, y_{i+1}) and point (x_{i-1}, y_{i-1}) on the wall; i.e.,

$$\Delta x_i = \frac{x_{i+1} - x_i}{2} + \frac{x_i - x_{i-1}}{2} = \frac{x_{i+1} - x_{i-1}}{2}$$

$$\Delta y_i = \frac{y_{i+1} - y_i}{2} + \frac{y_i - y_{i-1}}{2} = \frac{y_{i+1} - y_{i-1}}{2}$$

Also $d_i = \sqrt{\Delta x_i^2 + \Delta y_i^2}$ is the length of line segment formed by $(\Delta x_i, \Delta y_i)$; in other words, the line length d_i is assigned to node i. The boundary condition on the wall is the condition of no normal flux across the wall (called the slip condition). Thus, the normal fluid velocity V_n on the wall relative to the wall velocity must be zero, i.e.,

$$V_{ni} = 0$$

Received Oct. 31, 1994; revision received March 23, 1995; accepted for publication March 23, 1995.

*Professor, Institute of Aeronautics and Astronautics. Member AIAA.

†Graduate Student, Institute of Aeronautics and Astronautics; currently Associate Professor, National Tainan Teachers College, Tainan 701, Taiwan, Republic of China.

‡Associate Professor, Institute of Aeronautics and Astronautics. Member AIAA.

on the wall at node i, which is related to the fluid velocity (u_{wi}, v_{wi}) by the relationship

$$V_{ni} = -(u_w - \dot{x})_i \frac{\Delta y_i}{d_i} + (v_w - \dot{y})_i \frac{\Delta x_i}{d_i} = 0 \qquad (1)$$

The fluid tangent velocity V_t on the wall is obtained by extrapolation from the fluid velocities at interior points,

$$V_{ti} = (u_w - \dot{x})_i \frac{\Delta x_i}{d_i} + (v_w - \dot{y})_i \frac{\Delta y_i}{d_i} \qquad (2)$$

Solving Eqs. (1) and (2), we can determine the fluid velocity (u_w, v_w) on the wall. The pressure and density on the wall are also determined by extrapolation from interior points. When the wall has no deformation, $\dot{x}_i = \dot{y}_i = 0$, the flexible-wall boundary reduces to a rigid-wall boundary.

Upstream and Downstream Boundaries

The characteristic boundary conditions are imposed at upstream and downstream boundaries depending on whether the flow condition is subsonic or supersonic. For the transonic flow problem considered, the nozzle back pressure is prescribed at the nozzle exit.

Initial Condition

For a static aeroelastic problem, a steady-state solution with rigid walls is used as an initial guess. For an unsteady transonic aeroelastic problem with shock waves, a static aeroelastic solution is chosen as an initial condition.

Iterative Procedure for Aeroelastic Response

A step-by-step calculation is performed. Assuming a rigid wall first, the wall pressure is calculated by our flow solver. Next, the discrete spring model is employed to generate a new wall shape. For the new wall shape, the flowfield and the wall pressure are updated. The process is repeated until a steady aerodynamic flow and a static structural deformation are obtained at time t. The flow solution at time t is provided as an initial condition for computing the next flowfield at time $t + \Delta t$.

Choice of Time Step

For unsteady flow calculation, the time step Δt is chosen to be the minimum of $\Delta t(\xi, \eta)$ over the whole computation domain (ξ, η), where $\Delta t(\xi, \eta)$ denotes the product of the Courant number chosen and the minimum of the characteristic times along the ξ and η direction on all finite volumes.

Results and Discussion

Validation of Computer Code

To validate the present spring model for wall flexibility, the nozzle A2 used in the experiments of Mason et al.[2] is adopted. The nozzle shape is given in Fig. 1. Note that the dimensions of $\bar{X}$ and $\bar{Y}$ are in centimeters. The nozzle throat is located at $\bar{X} = 5.79$ cm. A grid system with 60×16 finite volumes, as shown in Fig. 1, was chosen in computing the steady-state (equilibrium) solution with given back pressure ratio of $p_b/p_t = 0.3367$, where p_t denotes the upstream total pressure. In this case, the flow is isentropic and is accelerated from subsonic at the entrance to supersonic at the exit. Since Felker's inviscid-flow solution[1] did not agree well with the test data of Mason et al., we felt that the deviation may be due to the neglect of viscous effects in Felker's model. To investigate this aspect we also computed the viscous flow in the channel with rigid walls at the same back pressure using the Navier–Stokes equations in conjunction with a thin-layer approximation.

The computed wall pressures are shown in Fig. 2 and compared to test data. It can been seen that the rigid-wall solution does not agree well with the experimental data and the flexible-wall solution does agree well with the test data. Moreover, the computed viscous-flow solution is not improved very much using the Navier–Stokes equations at the Reynolds number of 2000. Other Reynolds numbers from 200 to 20,000 were also tried, but no significant improvement could be obtained. It is concluded that the wall flexibility plays an important role in a transonic nozzle flow. Because of the structural outward deformation, the cross-sectional area of the flexible-wall nozzle was found to be larger than that for the rigid-wall nozzle. The maximum structure deformation was 3.3%, which occurred at the nozzle throat.

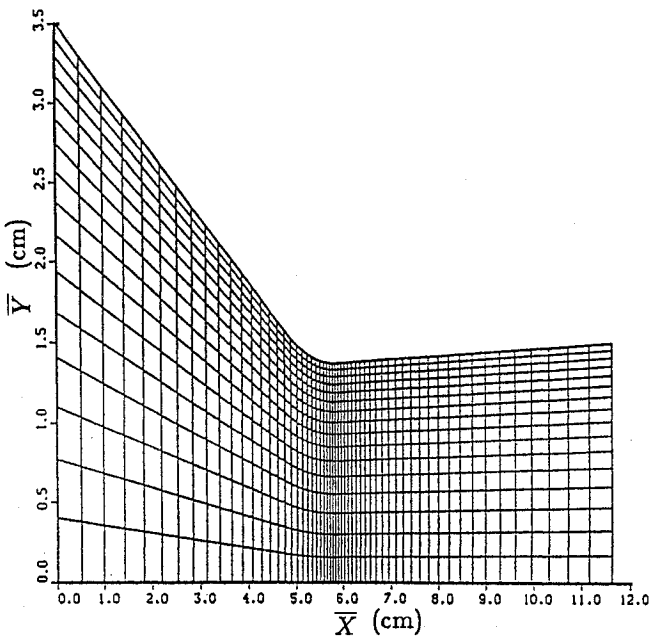

Fig. 1 Grid used for a two-dimensional convergent-divergent nozzle.

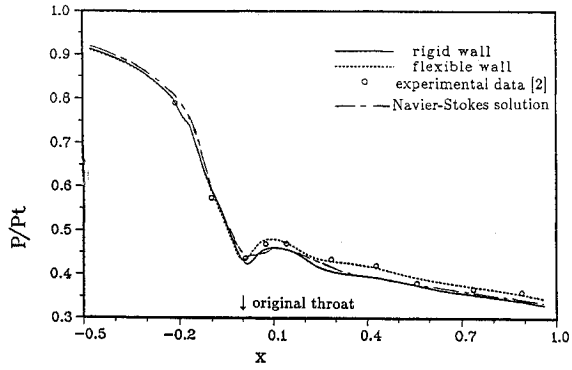

Fig. 2 Comparison of computed wall pressures with test data.

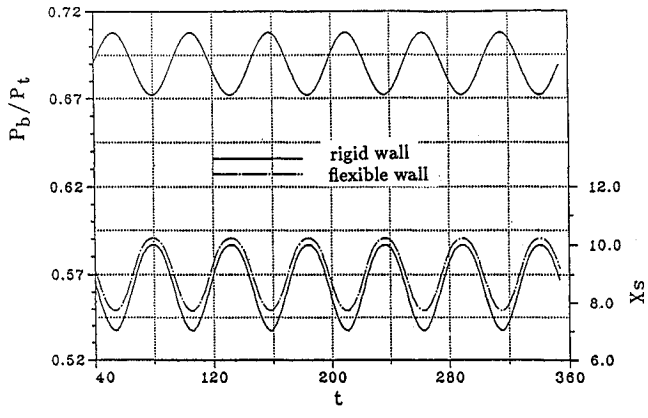

Fig. 3 Comparison of shock movements at the shock root in rigid- and flexible-wall nozzles.

Shock Oscillation in the Flexible-Wall Nozzle

With a steady transonic flow and a shock wave in the flexible-wall nozzle, the shock oscillation is induced by the introduction of a back pressure perturbation as

$$p_b(t) = p_{st} + \bar{p} \sin(\theta) \qquad \theta = \omega(t - t_0)$$

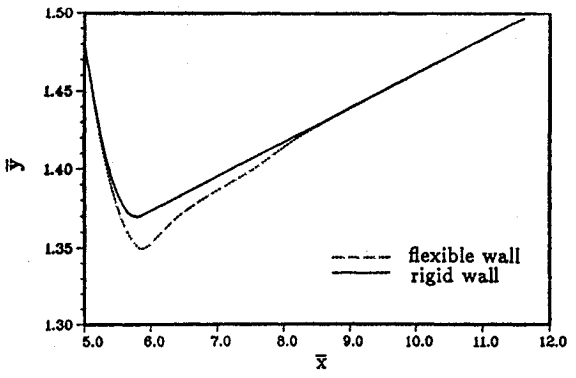

a) $\theta = 0, 2\pi$

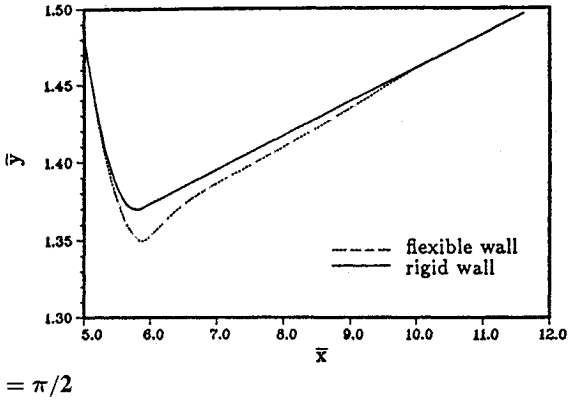

b) $\theta = \pi/2$

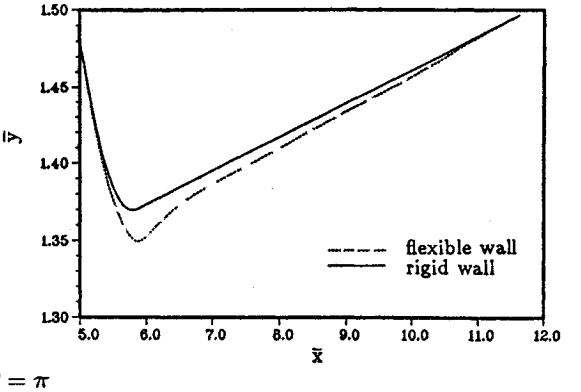

c) $\theta = \pi$

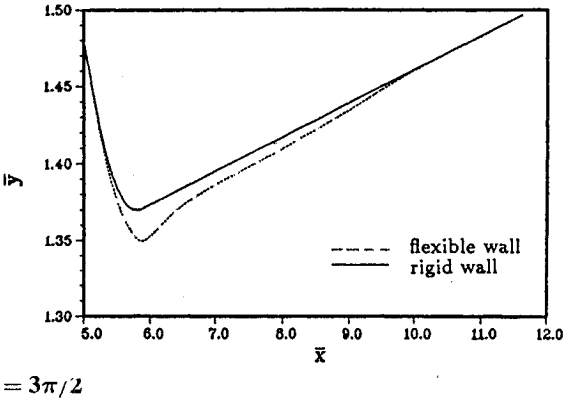

d) $\theta = 3\pi/2$

Fig. 4 Geometries of a flexible-wall nozzle at different instants.

where p_b is the back pressure, which has been normalized by the upstream total pressure p_t, p_{st} is the steady back pressure and set to be 0.69, $\bar{p}$ is the amplitude of the pressure perturbation, ω is the reduced frequency, t is the dimensionless time, and t_0 is set to be 40. In this study, we set $\bar{p} = 0.018$ and $\omega = 0.06$. In addition to the influence of the downstream pressure fluctuation, the shock oscillation can be affected by the wall flexibility. Figure 3 shows the comparison of shock movements at the shock root for the rigid- and flexible-wall cases. The shock amplitude is 1.24 cm in the flexible-wall nozzle and 1.48 cm for the rigid-wall case.

During one cycle of oscillation, the average shock position ($\bar{X}_{s,\text{ave}}$) at the shock root is $\bar{X}_{s,\text{ave}} = 8.94$ cm for the flexible-wall case, which is farther downstream than that ($\bar{X}_{s,\text{ave}} = 8.52$ cm) for the rigid-wall case. The shock amplitude at the location away from the shock root is larger than that at the shock root, as found in the rigid wall.[3] The shock amplitude at the centerline is found to be 1.28 cm for the flexible wall and 1.52 cm for the rigid wall. The average shock positions at the centerline for flexible and rigid walls are 9.02 and 8.57 cm, respectively.

Structural Deformation and Internal Flowfield

Owing to the interaction of the oscillating shock with the flexible wall, the wall geometry and internal flowfield are changed with time. Figures 4a–4d show the wall deformations at four different times indicated by $\theta = 0, \pi/2, \pi$, and $3\pi/2$, which correspond to $t = 66.2, 92.3, 118.5$, and 144.7. The corresponding flowfields of Mach number distributions at these times were also plotted, but not shown here because of space limitation. It was found that the flexible wall is deformed inward only from $\bar{X} = 5.3$ cm to $\bar{X} = 11$ cm approximately during an oscillation cycle, since the internal wall pressure over this region is lower than the reference pressure. At other locations the wall has no deformation. The maximum wall deformation is about 1.5%, which occurs at the throat, resulting in a nozzle with larger area ratios, compared to the rigid-wall case.

From Fig. 4 one can see the interaction of the aeroelastic and aerodynamic forces. When $\theta = 0$ and π, the downstream pressure is increasing, the shock wave is moving upstream, and the deformed region is being reduced. When $\theta = \pi/2$ and $3\pi/2$, the downstream pressure is decreasing, the shock wave is moving downstream, and the deformed region of the wall is being enlarged.

Larger Motion of Shock Wave

To obtain a larger motion of shock wave, p_{st} is changed from 0.69 to 0.712 and $\bar{p}$ from 0.018 to 0.04. In this case a steady shock is located near the throat if no pressure perturbation is introduced. When the downstream pressure is perturbed harmonically, the shock wave can move upstream, becoming a compressive wave, and reappears behind the throat. The geometric variations of the wall at different times can be obtained from the plots similar to Fig. 4. It was found that the throat is deformed inward, and the change in its cross-sectional area is about 1.8% when the flow is choked and about 1% when the shock wave disappears.

Conclusion

A spring model has been developed for representing wall flexibility and tested to be appropriate for calculating the nozzle flow with flexible walls. The present model has the advantage of structural stiffness being adaptive to grid spacing. It is found that the shock wave in transonic flows is greatly influenced by the wall flexibility and the downstream pressure perturbation. The interaction of the aeroelastic and aerodynamic forces in the flexible-wall nozzle has been successfully simulated and investigated in detail. The success of the two-dimensional flexible-wall nozzle problem is a stepping stone for three-dimensional aeroelastic nozzle problems.

Acknowledgment

The partial support for this study under National Science Council Contract NSC-81-FSP-006-04 is gratefully acknowledged.

References

[1]Felker, F. F., "Fully-Coupled Structural Deformations and Computational Fluid Dynamics: Direct Solution Using Newton's Method," *4th International Symposium on Computational Fluid Dynamics* (University of California at Davis, CA), Vol. 1, 1991, pp. 323–328.

[2]Mason, M. L., Putnam, L. E., and Re, R. J., "The Effect of Throat Contouring on Two-Dimensional Convergent-Divergent Nozzles at Static Conditions," NASA TP-1704, July 1980.

[3]Liang, S. M., and Tsai, C. J., "Shock Oscillation in Two-Dimensional Inviscid Unsteady Channel Flow," *AIAA Journal*, Vol. 31, No. 1, 1993, pp. 200–203.

[4]Guruswamy, G. P., "Unsteady Aerodynamic and Aeroelastic Calculations for Wings Using Euler Equations," *AIAA Journal*, Vol. 28, No. 3, 1990, pp. 461–469.
[5]Tsai, C. J., "A New Concept of Weighting on Schemes for Hyperbolic Equations with Application to Channel Flows," Ph.D. Dissertation, Inst. of Aeronautics and Astronautics, National Cheng Kung Univ., Tainan, Taiwan, ROC, June 1993.
[6]Yee, H. C., and Harten, A., "Implicit TVD Schemes for Hyperbolic Conservation Laws in Curvilinear Coordinates," *AIAA Journal*, Vol. 25, No. 2, 1987, pp. 266–274.
[7]Beam, R. M., and Warming, R. F., "An Implicit Factored Scheme for the Compressible Navier–Stokes Equations," *AIAA Journal*, Vol. 16, No. 4, 1978, pp. 393–402.

Effect of Transverse Shear on Aeroelastic Stability of a Composite Rotor Blade

Sung Nam Jung*
Chonbuk National University,
Chonju 560-756, Republic of Korea
and
Seung Jo Kim†
Seoul National University,
Seoul 151-742, Republic of Korea

Introduction

IN the analysis point of view, the composite rotor blade has typically been analyzed through the one-dimensional beam assumption since the spanwise length of rotor blades is generally much longer than their lateral dimensions. In developing the beam theory, there may be coupling among extension, bending, and torsional deformations. These couplings generally invalidate the Euler–Bernoulli assumption: plane sections remain plane and are perpendicular to the elastic axis. The assumption leads to underestimation of beam displacements, especially in case of bending, because of constant shear distribution across the beam section. Moreover, for a composite beam in bending, this distribution of shear is nearly parabolic (piecewise in general).[1] The use of the shear correction factor (SCF) may be the most economical one for the transverse shear behavior without largely sacrificing the required accuracy of solution. In addition, warping and warping inhibition effects are to be considered in the analysis.[2] Therefore, an appropriate analytical model capturing these behaviors is inevitable to get more enhanced results from the aeroelastic analysis of a composite rotor blade.

Hong and Chopra[3] used the nonlinear kinematic model of Hodges and Dowell[4] and extended it to the case of composite rotor. They used a simplified beam model, in which the transverse shear flexibility was not included in the formulation. Smith and Chopra[5] modified this one to include the transverse shear effects and other secondary structural modeling effects. They focused on the behavior of an elastically tailored composite blade and presented various results for vibratory hub loads of box-beam having different ply configurations, but they did not go further to consider the sectional distribution of shear stresses. To improve the theoretical results, an alternative approach, which has been developed by Jung and Kim[6] for the effects of transverse shear and structural damping on the aeroelastic response of composite rotor blades in hover, involved the usage of SCF to account for the sectional distribution of shear stresses. They showed that the effects of transverse shear and structural damping can have a key role on the flutter boundary of the rotor, but the lay-up structure is confined to symmetric configuration only. In the present work, the formulation of Ref. 6, which considers the effects of transverse shear flexibility, torsion warping, and two-dimensional in-plane behavior, is extended to analyze arbitrary lay-up geometry including antisymmetric configuration. Numerical simulations are performed for a specific antisymmetric configuration to identify the transverse shear behavior on the aeroelastic stability of composite rotor.

Received Sept. 16, 1994; revision received Feb. 6, 1995; accepted for publication Feb. 6, 1995.

*Full-Time Instructor, Department of Aerospace Engineering, Dukjin-Ku. Member AIAA.
†Associate Professor, Department of Aerospace Engineering, Kwanak, Ku. Member AIAA.

Problem Formulation

The rotor structure is idealized as a laminated composite box-beam whose constituent laminae are characterized by different ply orientation angles and different material and thickness properties as depicted in Ref. 6. The deformation of the blade in space is described by u, v, w, and ϕ, which are, respectively, axial, lead-lag, flap, and elastic twist deformations. The total transverse displacements of in-plane and out-of-plane bending are expressed as the sum of the displacement due to bending and the displacement due to shear deformation. The same kinematic relations and constitutive relations that are given by Ref. 6 for the composite box model are used in the present formulation. In case of thin-walled construction of box-beam, the internal shear stresses for the equivalent load applying at shear center are distributed in a form as shown in Fig. 1. Since the distribution of shear strain (or stress) in the load direction of the wall is shown to have nearly parabolic function,[1] an appropriate treatment for the distribution of shear is required for the one-dimensional beam kinematics. Based on the equivalent energy concept, the SCFs are introduced in the present beam formulation to describe the motion. The equilibrium relations for the box-beam composed of orthotropic laminates can be written in the form

$$\begin{Bmatrix} Q_\eta \\ Q_\zeta \end{Bmatrix} = \begin{bmatrix} k_{11}GA_h & 0 \\ 0 & k_{22}GA_v \end{bmatrix} \begin{Bmatrix} v_S' \cos\bar{\theta} + w_S' \sin\bar{\theta} \\ w_S' \cos\bar{\theta} - v_S' \sin\bar{\theta} \end{Bmatrix} \quad (1)$$

where the subscript s represents shear deformation, Q_η and Q_ζ are shear stress resultants in horizontal and vertical directions of box-beam, GA_h and GA_v are the respective shear moduli, k_{11} and k_{22} are the SCFs for in-plane and out-of-plane directions, respectively, and $\bar{\theta}$ is the total geometric pitch angle of blade.

The variation of strain energy δU for the composite blade can be written by

$$\delta U = \int_0^R \iint_A (\sigma_{xx}\delta\varepsilon_{xx} + \sigma_{x\eta}\delta\varepsilon_{x\eta} + \sigma_{x\zeta}\delta\varepsilon_{x\zeta})\, d\eta\, d\zeta\, dx \quad (2)$$

where σ and ε represent engineering stress and engineering strain components, respectively. Substituting the stress-strain and strain-displacement relations, which are described in Ref. 6, into the preceding strain energy equation, and taking Eq. (1) into account, one can obtain the variational form of the strain energy in terms of displacement components. In obtaining the expression of strain energy variation, an ordering scheme is used similar to Ref. 4 to

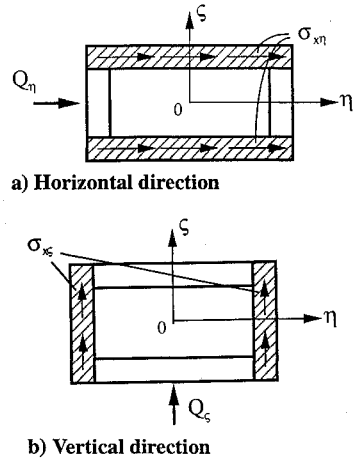

a) Horizontal direction

b) Vertical direction

Fig. 1 Distribution of shear stresses due to applied forces.